

Loop level lepton flavor violation at linear colliders

Mirco Cannoni

Dipartimento di Fisica, Università degli Studi di Perugia and INFN Sezione di Perugia,
Via A. Pascoli 1, 06123, Perugia, Italy
E-mail: mirco.cannoni@pg.infn.it

Oriando Panella and Stephan Kolb

INFN, Sezione di Perugia, Via A. Pascoli 1, 06123, Perugia, Italy

Abstract: We present a study of loop-level lepton flavor violating signals in models with heavy Majorana neutrinos and in the supersymmetric extension of the standard model. The attention is focused to the e^+e^- option of the next generation of linear colliders and its potential of discovering new physics is emphasized.

1. Introduction

Linear e^+e^- colliders are very important step towards the understanding of high energy particle interactions. Besides confirming and allowing precision measurements on new physics which, hopefully, will be discovered at the LHC, they offer by themselves new physics opportunities thanks to the possibility of e^+e^- , $e^+e^+e^-$ collisions. These options will allow to test, with higher sensitivity couplings of the standard model (and alternative theories) which cannot be studied in hadronic or e^+e^- collisions. Moreover the possibility of employing electron beam with a high degree of longitudinal polarization will be essential to enhance signals of new physics.

The e^+e^- mode with lepton number $L = +2$ of the initial state is particularly suitable for studying lepton and flavor number violating reactions (LFV). The merits of this option have been recently recalled by the ECFA/DESY working group in Ref. [1]. Among these there is (1) the possibility to identify Majorana neutrinos of masses in the TeV range through the "inverse neutrinoless double beta decay" reaction $e^+e^- \rightarrow W^+W^-$, and (2) the sharper onset of slepton production threshold respect to the e^+e^- option. Here we present a study of two loop-level reactions strictly connected with these two merits: we first consider seesaw type models with heavy Majorana neutrinos at the TeV scale and

Speaker.

study the reactions $e e \rightarrow \nu \nu$, and then similar reactions $e e \rightarrow \nu e$ ($\nu = \mu, \tau$) in supersymmetric models where LFV is due to slepton mixing.

We briefly discuss the standard model background. More details on the calculations and numerical tools used can be found in Refs. [2, 3].

2. $e e \rightarrow \nu \nu$ ($\nu = \mu, \tau$) through heavy Majorana neutrinos

To give a detectable signal, heavy Majorana neutrinos (HMN), besides having masses in the TeV range, must have interactions which are not suppressed by the mixing matrices with light states as instead happens in the one family seesaw mechanism, where $\frac{P}{m} \approx M_N$. With three generations, more free parameters are at our disposal, and the "two miracles" of not so large masses and non negligible mixing, are obtained imposing suitable relations among the elements of the matrices m_D and M_R : examples of these models were proposed some time ago in Refs. [4, 5, 6] and in the more recent paper, Ref. [7], whose authors suggest "neutrinos" as the correct name for these particles. According to other authors, Ref. [8], these models are based on fine-tuned relations, but are shown to be not in contradiction with any experimental bound. We do not enter in such a theoretical dispute and assume "neutrinos" in the TeV range and study the phenomenological consequences.

Experimentally one cannot put bounds on the single mixing matrix elements, but on some combinations of them, assuming that each charged lepton couples only to one heavy neutrino with significant strength. Light-heavy mixing has to be inferred from low-energy phenomenology and from global tests performed on LEP data identifying the following effective mixing angles $s_e^2 = \frac{P}{j} B_{iN_j}^2 \sin^2 \theta$, with upper bounds [9]:

$$s_e^2 < 0.0054; \quad s^2 < 0.005; \quad s^2 < 0.016; \quad (2.1)$$

where B is the mixing matrix appearing in the charged current weak interaction Lagrangian. Under these assumptions, the coupling of neutrinos to gauge bosons and leptons is numerically fixed to $g B_{N_i}$, where g is the SU(2) gauge coupling of the SM. Since the width of the heavy states grows as M_N^3 , at a certain value it will happen that $\Gamma_N > M_N$, signaling a breakdown of perturbation theory. The perturbative limit on M_N is thereby estimated requiring $\Gamma_N < M_N = 2$, which gives an upper bound of ≈ 3 TeV [10] for the numerical values given in Eq. (2.1).

We study the process $e e \rightarrow \nu \nu$ ($\nu = \mu, \tau$), which violates the L_e and L_ν lepton numbers. The amplitudes are computed in the 't Hooft-Feynman gauge where there are graphs with $W W$, γW and W exchange, γ being the Goldstone boson, as shown in Fig. 1. The numerical computation of the four-point functions was performed using the loop-tools [11] package. A similar study was done in Ref. [12] using the approximation where all external momenta in the loops are neglected relative to the heavy masses of the gauge bosons and Majorana neutrinos, that is $q_i = k + k_i \approx k$, where k is the integration variable in the loop integrals and k_i are the sums of external momenta appearing in the propagators. This approximation for the four-point functions is good at low energies, such as in decay processes of heavy mesons, or when $\frac{P}{s} \ll M$, M being the highest mass running in the loop. In this way the cross section presents a linear growth with s which breaks

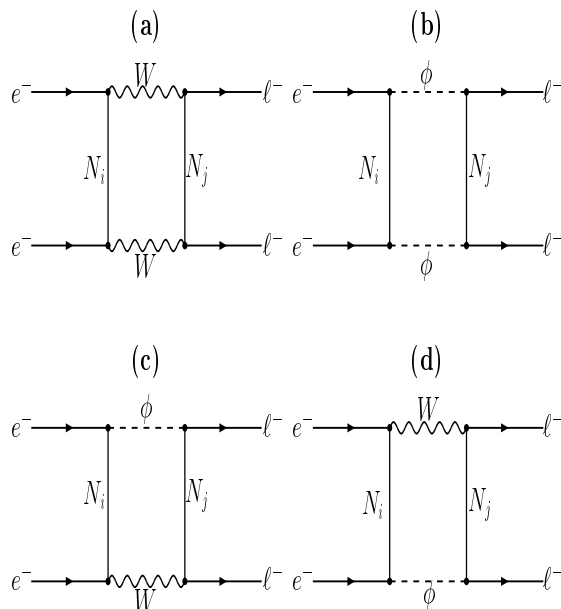


Figure 1: In (a-d) the Feynman diagrams, in the 't Hooft-Feynman gauge, contributing to $e^- e^- \rightarrow \ell^- \ell^-$ ($\ell = e, \mu$) via heavy Majorana neutrinos. ϕ is the unphysical Goldstone boson.

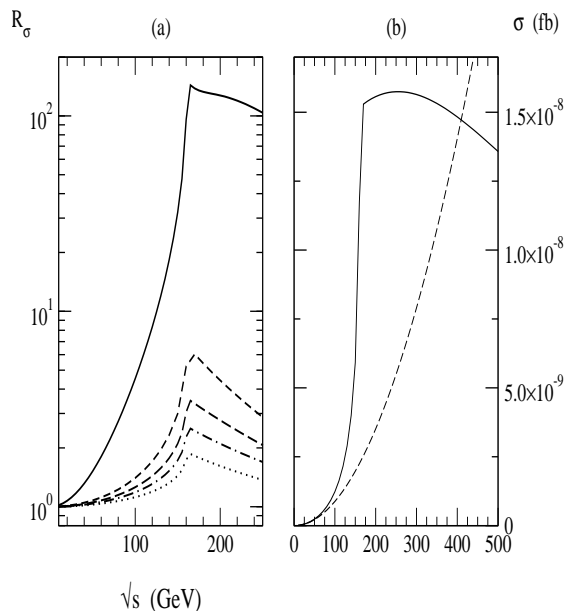


Figure 2: (a) the ratio R_σ is plotted as a function of \sqrt{s} . Solid line, $M_{N_i} = M_{N_j} = 100$ GeV; dotted, $M_{N_i} = M_{N_j} = 3$ TeV. (b) Solid line, our calculation, dashed line that of Ref. [12].

unitarity: therefore, in order to make quantitative predictions with the correct high energy behavior, full dependence on the external momenta of the four-point functions has to be considered. Theoretically, according to the Cutkosky rule, one expects an enhancement at $\sqrt{s} \approx 161$ GeV $\approx 2M_W$, the threshold for on-shell W^+W^- gauge boson production, at which the four-point functions develop an imaginary part. In Fig. 2 (a) the ratio $R_\sigma = \sigma_{\text{tot}} / \sigma_{\text{tot}}|_{\text{low}}$ of the integrated total cross section to the cross section of the low energy calculation of Ref. [12], is plotted for sample values of the Majorana masses. The enhancement due to the threshold singularity of the loop amplitude is more pronounced for values of Majorana masses close to M_W and is drastically reduced increasing $M_{N_i} = M_{N_j}$ to O (TeV). As $R_\sigma \rightarrow 1$ at $\sqrt{s} \ll M_W$ in all the cases, the agreement of our full calculation with the result of Ref. [12] in the regime of low energies is evident. The threshold effect appears to be quite spectacular only for values of Majorana masses which correspond to cross sections too small to be measured even at a next linear collider. In Fig. 2 (b) the effect of the threshold singularity in the loop integral is shown reporting absolute cross sections for a particular choice of Majorana masses: $M_{N_i} = 150$ GeV and $M_{N_j} = 450$ GeV. The low energy approximation (dashed line), obtained neglecting external momenta in the loop, is inadequate when the energy of the reaction increases to values comparable with the masses. Increasing the energy, after reaching a maximum, the cross section starts to decrease until the asymptotic behaviour $\mathcal{O}(1/s^2)$ of the loop integral is reached. This happens for every value of heavy Majorana neutrino masses and we checked numerically that, as expected, for higher masses the asymptotic regime is reached at higher values of \sqrt{s} . In fact from Fig. 3

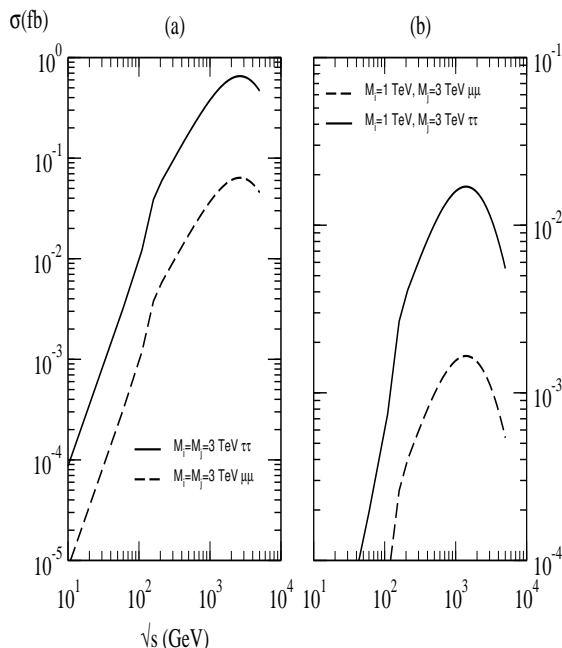


Figure 3: Total cross sections as function of \sqrt{s} . (a) the solid curve refers to the case of $(e^+e^-) \rightarrow \tau^+\tau^-$ with $M_{N_i} = M_{N_j} = 3$ TeV, while the dashed line refers to $(e^+e^-) \rightarrow \mu^+\mu^-$ with the same values of Majorana masses. (b) the Majorana masses are changed to somewhat lower values: $M_{N_i} = 1$ TeV, $M_{N_j} = 3$ TeV.

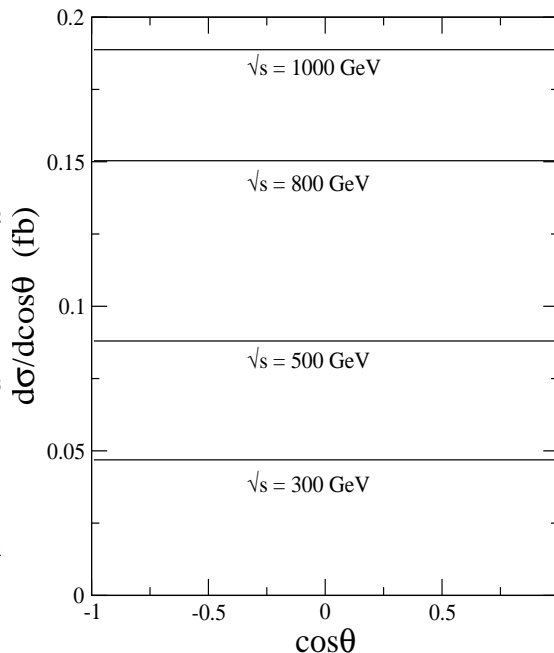


Figure 4: Angular distribution in the polar angle of the outgoing lepton for different values of the center of mass energy, \sqrt{s} in the case of $(e^+e^-) \rightarrow \tau^+\tau^-$ with $M_{N_i} = M_{N_j} = 3$ TeV. The curves are not exactly constant, and using an appropriate scale they show small deviations from a straight line, remaining left-right symmetric.

we note that the cross section grows with increasing HMN masses. The main contribution comes from the graph with two Goldstone bosons since their coupling is proportional to M_{N_i} . Moreover the chiral structure of the coupling selects the mass term in the numerator of the Majorana neutrino propagators. When these masses are much larger than the other quantities, the amplitude scales like $M_{N_i}^3 M_{N_j}^3 = M_{N_i}^2 M_{N_j}^2 \cdot M_{N_i} M_{N_j}$, i.e. is proportional to the square of the heavy masses. This fact is the well known non decoupling of heavy fermions in theories with spontaneous symmetry breaking (similarly in the SM the top quark gives sizable radiative corrections owing to its large mass and a quadratic non decoupling). In Fig. 3 (a) the cross section is plotted for masses up to the perturbative limit, using the maximally allowed value of the mixing. We see that for $M_{N_i} = M_{N_j} = 3$ TeV the signal does reach the level of $10^{-1}; 10^{-2}$ fb respectively for the $(\tau^+\tau^-)$ and the $(\mu^+\mu^-)$ signals at $\sqrt{s} = 500$ GeV, which for an annual integrated luminosity of 100 fb^{-1} would correspond respectively to 10 and 1 event/year. At higher energies, O (TeV), one could get even larger event rates (30 and 3) respectively. The solid curve refers to $(e^+e^-) \rightarrow \tau^+\tau^-$: this is largest because the upper limits on the mixing are less stringent. One can also see the onset of the asymptotic regime at $\sqrt{s} = 3$ TeV. Fig. 3 (b) shows that the cross section quickly decreases as lower Majorana masses are considered.

As even in the more optimistic cases event rates are quite modest it is important to

check how the signal cross-section is affected by kinematic cuts on the angle of the outgoing leptons. The angular distributions turn out to be practically constant as shown in Fig. 4. They are forward-backward symmetric because both the t and u channel are present. The absence of a strong dependence on the polar angle is due to the fact that within the range of the parameters used here the contributing four point functions depend very mildly on the kinematic variables (u and t). This behaviour can be most easily understood using helicity amplitudes. In the limit of massless external particles the process is dominated by a well defined helicity amplitude: $e_L e_L \rightarrow \nu_L \nu_L$. In the center of mass frame this is a S -wave scattering with $J_z = 0$, meaning that the scattered particles are emitted back to back but without a preferred direction relative to the collision axis (z). Thus this signal is characterized by practically flat angular distributions and as a result the total cross section is quite insensitive to angular cuts. We have verified that with $\cos \theta_j \geq 0.99$ the change in σ_T is 1% for all energies considered, while using $\cos \theta_j \geq 0.95$ the total cross-section decreases by 5%. The reduction of the total cross section is measured almost precisely by the reduction of the phase space, meaning that the angular distribution is constant up to 0.1%. Thus it can be concluded that the number of events will not be drastically affected for any reasonable choice of experimental cuts. The possibility of employing electron beams with a high degree of longitudinal polarization as planned for the new colliders will be essential to discover rare signals: in our case only an helicity amplitude contribute, so that using left-polarized electron beams will single out the essential spin configuration and we can gain a factor ~ 4 on the previous cross sections, because the average on the initial spins is not needed. This consideration applies also in the next Section.

3. $e e \rightarrow \nu e$ ($\nu = \mu, \tau$) in R -conserving supersymmetric models

Slepton and squark mass matrices in soft-breaking potential, for example $m_{\tilde{L}}^2$, are in general complex non-diagonal matrices. The diagonalization implies the presence of generational mixing matrices at the lepton-slepton-gaugino vertices. These couplings can originate too high rates for rare unobserved flavor changing processes. The SUGRA boundary conditions and the renormalization group equations (RGE) evolution originate flavor-diagonal sfermion mass matrices, so besides offering a mechanism for reducing to a manageable number the soft parameters, also cure the 'flavor problem'. On the other hand, if one wants to study the phenomenology of the MSSM without referring to a particular high energy scenario, one can consider general mass matrices and accept their flavor violating entries as large as the experimental bounds allow them.

However when the seesaw mechanism is embedded in the MSSM with SUGRA boundary conditions at high energy and heavy Majorana neutrinos are out of the colliders reach, a new source of LFV arises. The seesaw mechanism requires that the superpotential contains three $SU(2)_L$ singlet neutrino superfields \hat{N}_i with the following couplings [13, 14]:

$$W = (Y)_{kl} \hat{H}_2^i \hat{N}_k \hat{L}_l^j + \frac{1}{2} (M_R)_{ij} \hat{N}_i \hat{N}_j \quad (3.1)$$

Here H_2 is a Higgs doublet superfield, L_i are the $SU(2)_L$ doublet lepton superfields, Y is a Yukawa coupling matrix and M_R is the $SU(2)_L$ singlet neutrino mass matrix. With the

additional Yukawa couplings in Eq. (3.1) and a new mass scale (M_R) the RGE evolution of the parameters is modified. Assuming that M_R is the mass scale of heavy right-handed neutrinos, the RGE evolution from the GUT scale down to M_R induce off-diagonal mass elements in $(m_L^2)_{ij}$. At the GUT scale we assume the universal conditions $m_L^2 = m_{\tilde{L}}^2 = m_{H_2}^2 = m_0^2$ and $A = a_0 Y$, thus the correction of the off-diagonal elements are (in the leading-log approximation):

$$(m_L^2)_{ij} \simeq \frac{1}{8} (3 + a_0^2) m_0^2 (Y^{YY})_{ij} \ln \frac{M_{GUT}}{M_R}; \quad (3.2)$$

which depends crucially on the non-diagonal elements of $(Y^{YY})_{ij}$, the square of the neutrino Yukawa couplings. The main point is that these elements can be large numbers because in the seesaw mechanism they do not directly determine the mass of the light neutrino, but only through the seesaw relation $m_D^2 = M_R = v^2 Y^2 = M_R$. On the other hand the same effect on the mass matrix of $SU(2)_L$ singlet charged sleptons $(m_R^2)_{ij}$ is smaller: in fact in the same leading-log approximation of Eq. (3.2), the corresponding RGE do not contain terms proportional to Y^{YY} , since the right-handed leptons fields have only the Yukawa coupling Y , which completely determines the Dirac mass of the charged leptons and these are known to be small numbers. Thus the off-diagonal elements $(m_R^2)_{ij}$ can be taken to be $\simeq 0$. The slepton mass eigenstates are obtained diagonalizing the slepton mass matrices. The corresponding mixing matrices induce LFV couplings in the lepton-slepton-gaugino vertices $\tilde{\chi}_{L_i} U_{L_{ij}} \tilde{L}_j$. The magnitude of LFV effects will depend on the RGE induced non diagonal entries and ultimately on the neutrino Yukawa couplings $(Y)_{ij}$.

The rate of LFV transitions like $\tilde{\nu}_i \rightarrow \tilde{\nu}_j, i \neq j, \tilde{\nu} = e, \mu$; induced by the lepton-slepton-gaugino vertex is determined by the mixing matrix $U_{L_{ij}}$ which, as stated above, is model dependent. In a model independent way, however, one can take the lepton, slepton, gaugino vertex flavor conserving with the slepton in gauge eigenstates, so that LFV is given by mass insertion of non diagonal slepton propagators. In a similar spirit our phenomenological approach will be quite model independent and, in order to keep the discussion simple enough, the mixing of only two generations will be considered. Thus the slepton and sneutrino mass matrix are:

$$m_L^2 = \begin{pmatrix} m^2 & m^2 \\ m^2 & m^2 \end{pmatrix}; \quad (3.3)$$

with eigenvalues: $m^2 = m^2 \pm m^2$ and maximal mixing matrix. Under these assumptions the LFV propagator in momentum space for a scalar line is

$$h_{ij}^{\tilde{\nu}} = \frac{i}{2} \frac{1}{p^2 - m_+^2} - \frac{1}{p^2 - m^2} = i \frac{m^2}{(p^2 - m_+^2)(p^2 - m^2)}; \quad (3.4)$$

and the essential parameter which controls the LFV signal is

$$LL = \frac{m^2}{m^2}; \quad (3.5)$$

In this scenario we consider the reaction

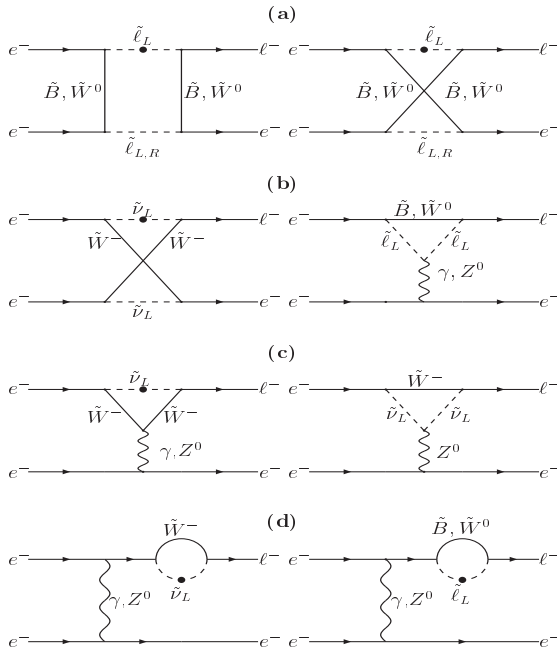


Figure 5: Feynman diagrams for e^-e^- collisions. The full black dot in a scalar line denotes again the lepton flavour violating propagator. Exchange diagrams are not shown.

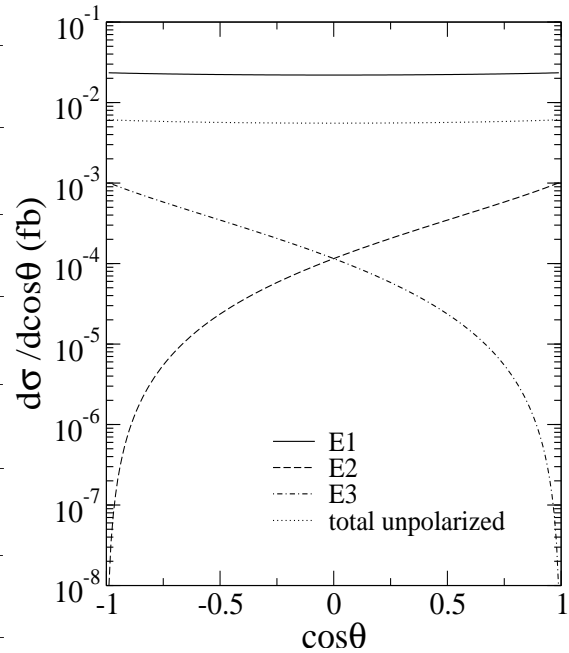


Figure 6: Differential cross sections as a function of the scattering angle. Values of the parameters: $M_1 = 80$; $M_2 = 160$; $m_{\tilde{\nu}_L} = m_{\tilde{\nu}_R} = 100$ GeV and $m_{\tilde{g}}^2 = 6000$ GeV².

$$e(p_1; \lambda_1) e(p_2; \lambda_2) \rightarrow e(p_3; \lambda_3) e(p_4; \lambda_4) \quad (3.6)$$

whose Feynman diagrams are shown in Fig. 5. Here λ_i denotes the helicity of particle i . The total unpolarized cross-section (averaged over initial spins) is $\sigma = \frac{1}{4} \sum_{\lambda_i} \sigma_{\lambda_i}$. The signal is suppressed if neutralinos and charginos $\tilde{\chi}^0$ are Higgsino-like, since their coupling is proportional to the lepton masses. For the same reason left-right mixing in the slepton matrix is neglected. Therefore it is assumed that the two lightest neutralinos are pure Bino and pure Wino with masses M_1 and M_2 respectively, while charginos are pure charged Winos with mass M_2 , M_1 and M_2 being the gaugino masses in the soft breaking potential. Numerical results are obtained using the mSUGRA relation $M_1 = 0.5M_2$ for gaugino masses while $m_{\tilde{g}}^2$ and the slepton masses are taken to be free phenomenological parameters. The parameter space is scanned in order to identify the regions which may deliver an interesting signal. The contributing amplitudes are

$$\begin{aligned} M_{E1} &= M(e_L e_L \rightarrow \tilde{\nu}_L e_L); \\ M_{E2} &= M(e_L e_R \rightarrow \tilde{\nu}_L e_R); \\ M_{E3} &= M(e_R e_L \rightarrow \tilde{\nu}_L e_R); \end{aligned} \quad (3.7)$$

The corresponding differential cross sections are plotted in Fig. 6. M_{E1} has $J_z = 0$, is flat and forward-backward symmetric because of the antisymmetrization. M_{E2} and M_{E3} describe P-wave scattering with $J_z = +1$ and $J_z = -1$ respectively: in order to conserve angular momentum M_{E2} must be peaked in the forward direction while M_{E3} favours backward scattering. Both M_{E2} and M_{E3} are orders of magnitude smaller than M_{E1} .

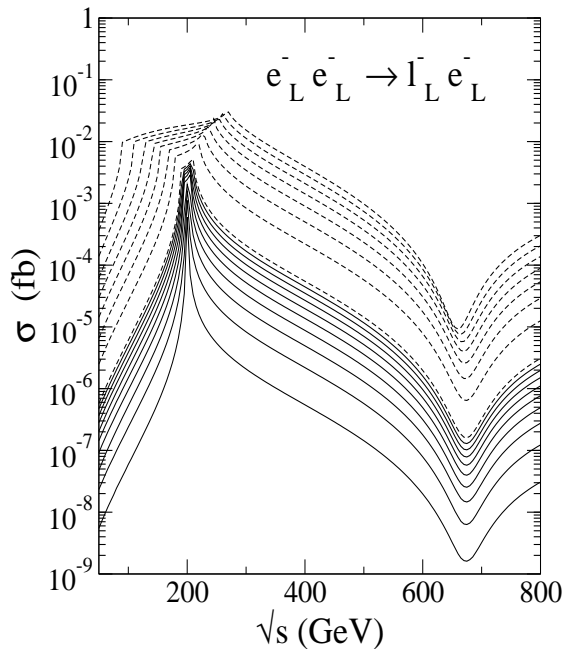


Figure 7: σ_{E1} as a function of \sqrt{s} with slepton and gaugino masses as in Fig. 6. Solid lines: m_L^2 increasing from 100 GeV^2 to 900 GeV^2 in steps of 100. Dashed lines: from 1000 to 8000 GeV^2 in steps of 1000.

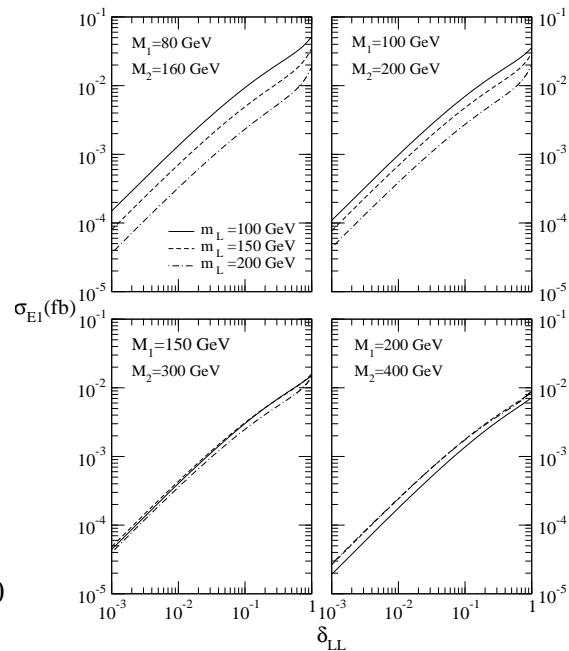


Figure 8: Total cross section for the amplitude $E1$ in function of δ_{LL} for $\sqrt{s} = 2m_L$. The values of the other parameters are given in the legends.

The signal cross section is to a very good approximation given by the amplitude M_{E1} . Since it is almost isotropic at the angular integration will give a factor almost exactly equal to two. This again shows the importance of the option of having polarized beams. If both colliding electrons are left-handed one singles out the dominant helicity amplitude and a factor four is gained in the cross section relative to the unpolarized case. This may be important in view of the relatively small signal cross section one is dealing with. The analysis of the total cross section as a function of \sqrt{s} is the following (see Fig. 7): the box diagrams dominate at $\sqrt{s} = 2m_L$ where m_L changes of orders of magnitude giving a sharp peak that is smeared only by large values of m_L^2 , while penguin diagrams give a substantial contribution only at higher energies. This can be easily understood considering the threshold behavior of the cross section for slepton pair production [15]: defining $\beta = \sqrt{1 - 4m_L^2/s}$ is the selectron velocity, the amplitude of the intermediate state $e_L^- e_L^- \rightarrow e_L^- e_L^-$ behaves like β , while for the other two cases it goes like β^3 . The dependence of σ_{E1} on δ_{LL} is shown in Fig. 8. With SUSY masses not much larger than 200 GeV the signal is of order $O(10^{-2}) \text{ fb}$ for $\delta_{LL} > O(10^{-1})$. In addition the cross section is practically angle independent and thus insensitive to angular (or transverse momentum) cuts.

The phenomenological points of the SUSY parameter space corresponding to gaugino masses $(M_1; M_2) = (80; 160) \text{ GeV}$ or $(100; 200) \text{ GeV}$ and to slepton masses $m_L = 100 - 200 \text{ GeV}$ and $\delta_{LL} > 10^{-1}$ (which implies $m_L^2 > 10^3 \text{ GeV}^2$) can give in the $e^- e^-$ mode a detectable LFV signal ($e^- e^- \rightarrow l^- e^-$) although at the level of $O(1 - 25)$ events/yr

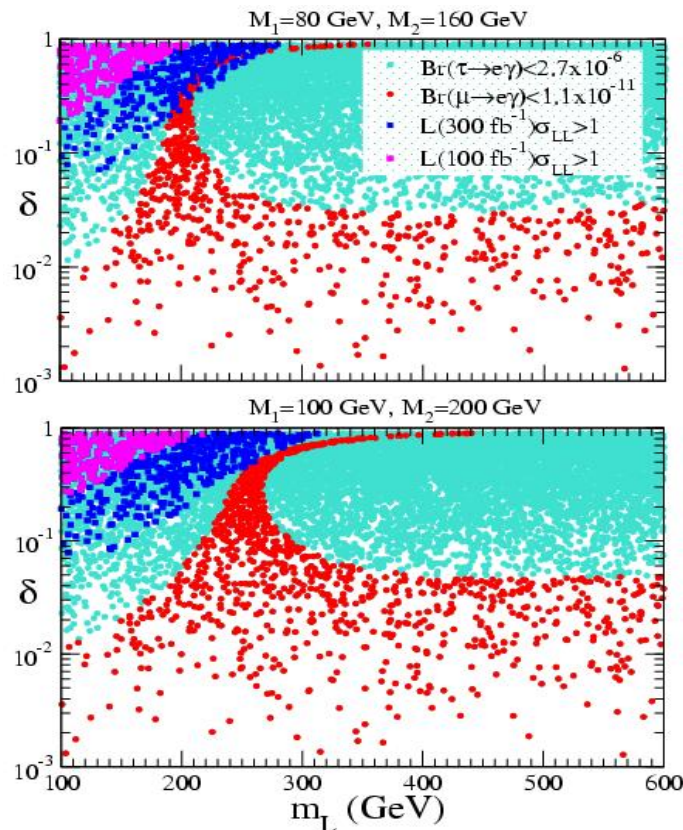


Figure 9: Scatter plot in the plane $(\sigma_{LL}; m_L)$ of: (a) the experimental bounds from $\tau \rightarrow e\gamma$ and $\mu \rightarrow e\gamma$ (allowed regions with circular dots); (b) regions where the signal can give at least one event with two different values of integrated luminosity (squared dots), for two sets of gaugino masses. Each signal point is calculated at $\sqrt{s} = 2m_L$.

with $L_0 = 100 \text{ fb}^{-1}$. Higher sensitivity to the SUSY parameter space could be obtained with larger L_0 . It is interesting to note that this light sparticle spectrum, which is promising for collider discovery, is also preferred by the electroweak data fit. In Ref. [17] it is shown that light sneutrinos, charged left sleptons and light gauginos improve the agreement among the electroweak precision measurements and the lower bounds on the Higgs mass. On the other hand the experimental bounds on rare lepton decays $\tau \rightarrow e\gamma$ set constraints on the LFV violating parameters m^2 or σ_{LL} : the upper bounds on the branching ratios define an allowed (and an excluded) region in the plane $(\sigma_{LL}; m_L)$ which are computed using the formulas given in Ref. [14] (adapted to our model) for the LFV radiative lepton decays. These regions have to be compared with those satisfying the "discovery" condition

$$L_0 (\sigma_{LL}; m_L) \geq 1 \tag{3.8}$$

Such a comparison is shown in Fig. 9 from which it emerges that: (i) For the $\tau \rightarrow e\gamma$ process there is an observable signal in the upper left corner of the $(\sigma_{LL}; m_L)$ plane. The extension of this region depends on L_0 . (ii) The bound from $\mu \rightarrow e\gamma$ does not constrain the region of the $(\sigma_{LL}; m_L)$ plane compatible with an observable LFV signal and therefore the

reaction $e e \rightarrow \nu \nu$ could produce a detectable signal within the highlighted regions of the parameter space (upper-left regions in the $(\sqrt{s}; m_L)$ plane). (iii) As regards the constraints from the $\nu \nu$ decay the allowed region in the $(\sqrt{s}; m_L)$ plane is shown by the circular dark dots (red with colour): the process $e e \rightarrow \nu \nu$ is observable only in a small section of the parameter space since the allowed region from the $\nu \nu$ decay almost does not overlap with the collider "discovery" region except for a very small fraction in the case of gaugino masses ($M_1 = 80 \text{ GeV}$ and $M_2 = 160 \text{ GeV}$). The compatibility of values of $\sqrt{s} = 1$ is due to a cancellation among the diagrams that describe the $\nu \nu$ decay in particular points of the parameter space.

4. Standard model background

These signals have the unique characteristic of a back to back high energy lepton pair and no missing energy. Sources of background were qualitatively discussed in Ref. [6]. Here we discuss the reaction $e e \rightarrow e e W W$ followed by the decays $W W \rightarrow \nu \nu \nu \nu$, with four neutrinos and a like sign-dilepton pair that can be of the same or different flavour. This appears to be the most dangerous background, as it produces two leptons and missing energy, and therefore it is analyzed in more detail.

Figure 10 shows the total cross section $e e \rightarrow e e W W$ calculated with the Com-
pHEP package [16], that allows to compute numerically the 17 Feynman diagrams contributing at tree level. Above the threshold for $W W$ gauge boson production the cross section rises rapidly by orders of magnitude, becoming almost constant at high energies. In the region $\sqrt{s} \approx 250 - 400 \text{ GeV}$ it increases from 10^{-2} fb to 1 fb . In order to get an estimate of the cross section for the six particle final state process, the cross section ($e e \rightarrow W W$) has to be multiplied by the branching ratio of the leptonic decays of the two gauge bosons, $\approx 10\%$, so that $\sigma_{\text{background}} \approx 10^{-4} - 10^{-2} \text{ fb}$, and it is at the level of the signal. However the kinematical configuration of the final state leptons is completely different. Figure 10 (upper-right) shows the angular distribution of the gauge bosons which is peaked in the forward and backward directions so that the leptons produced by the W gauge boson decay are emitted preferentially along the collision axis. In addition their transverse momenta will be softer compared to that of the signal: Fig. 10 (bottom-left panel) shows that the transverse momenta distribution of the gauge bosons is peaked at $p_T^p = (\sqrt{s} = 2 M_W) \approx 35 \text{ GeV}$ for $\sqrt{s} = 300 \text{ GeV}$. Consequently the lepton distributions will be peaked at $p_T^p \approx 17.5 \text{ GeV}$. The missing energy due to the undetected neutrinos (Fig. 10, bottom-right panel) can be as large as $\sqrt{s} - 2 M_W$. This distribution should be convoluted with that of the neutrinos produced in the gauge boson decay. Therefore it can be safely concluded that it will be possible to control this background because, with reasonable cuts on the transverse momenta of the leptons and on the missing energy, it will be drastically reduced, while – as mentioned above – these cuts will not affect significantly the signal. The same conclusion holds for the signal with heavy Majorana neutrinos: for $\sqrt{s} > 700 \text{ GeV}$ ($\approx 2 M_W$) is 10 fb , the six particles final state has very large missing energy carried away by neutrinos and charged leptons have soft distributions in transverse

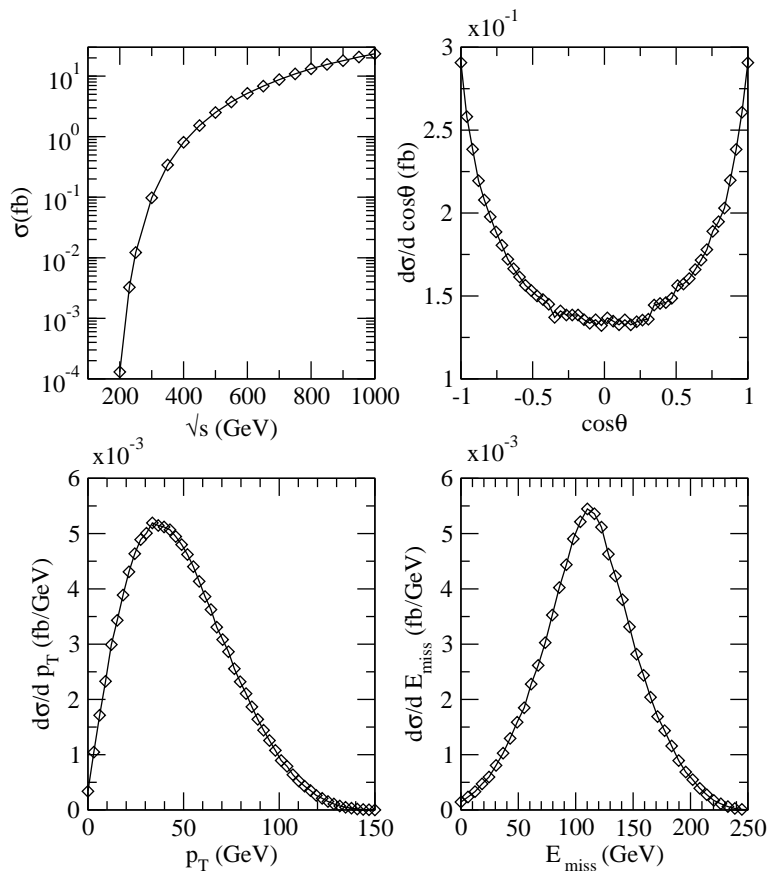


Figure 10: Total cross section and distributions for $e^+e^- \rightarrow W^+W^-$. Upper-left figure: total cross section as a function of \sqrt{s} . Upper-right: angular distribution for a W^- where θ is the angle among the collision axis and the boson momentum. Bottom-left: distribution of the transverse momentum of W^- . Bottom-right: energy distribution of the two neutrinos. All distributions are calculated with $\sqrt{s} = 300$ GeV.

momentum, thus cuts on missing energy and on the leptons p_T reduce the background but not the signal.

5. Conclusions

The e^+e^- option of the next generation of linear colliders offers the opportunity to test models of new physics through the discovery of lepton flavor violating signals, even if they arise only as a pure loop-level effect. We have shown, using the maximum experimentally allowed mixings, that masses of heavy Majorana neutrinos up to $2-3$ TeV can be explored with the reaction $e^+e^- \rightarrow \nu^+\nu^-; (\nu = \mu, \tau)$, because the amplitude gets an enhancement at the threshold for two gauge bosons production and then shows a non-decoupling behaviour with the mass of the virtual heavy states. For the similar reaction $e^+e^- \rightarrow \nu^+e^-; (\nu = \mu, \tau)$ induced by slepton mixing in supersymmetric models, in certain regions of the parameter space, the signal can reach the level of 10^{-2} fb around the threshold for selectrons pair production. The possibility of employing beams with high degree of longitudinal polarization

PRHEP AHHEP2003

is also essential to enhance the signal. On the other hand the standard model background is low and can be easily controlled.

Acknowledgments

M. C. thanks the organizers of AHEP 2003 Conference in Valencia for the financial support which allowed his participation. The work of S. K. at INFN-Perugia in the period 2001-2002 has been supported by European Union under the Contract No. HPMF-CT-2000-00752.

References

- [1] A. De Roeck, hep-ph/0311138
- [2] M. Cannoni, S. Kolb and O. Panella, Eur. Phys. J. C 28 (2003) 375, hep-ph/0209120
- [3] M. Cannoni, S. Kolb and O. Panella, Phys. Rev. D 68 (2003) 096002, hep-ph/0306170
- [4] W. Buchmüller and C. Greub, Nucl. Phys. B 363 (1991) 345
- [5] L. N. Chang, D. Ng and J. N. Ng, Phys. Rev. D 50 (1994) 4589, hep-ph/9402259
- [6] C. A. Heusch and P. Minkowski, Nucl. Phys. B 416 (1994) 3
- [7] W. Loinaz, N. Okamura, S. Rayyan, T. Takeuchi and L. C. R. Wijewardhana, Phys. Rev. D 68 (2003) 073001, hep-ph/0304004
- [8] J. Gluza, Acta Phys. Polon. B 33 (2002) 1735, hep-ph/0201002
- [9] E. Nardi, E. Roulet and D. Tommasini, Phys. Lett. B 327, 319 (1994); Phys. Lett. B 344, 225 (1995).
- [10] J. I. Illana and T. Riemann, Phys. Rev. D 63 (2001) 053004, hep-ph/0010193
- [11] T. Hahn and M. Perez-Victoria, Comput. Phys. Commun. 118 (1999) 153, <http://www.feynarts.de/loopools>
- [12] X. Y. Pham, Phys. Lett. B 495 (2000) 131, hep-ph/0003077
- [13] F. Borzumati and A. Masiero, Phys. Rev. Lett. 57 (1986) 961
- [14] J. Hisano, T. Mori, K. Tobe, M. Yamaguchi, Phys. Rev. D 53 (1996) 2442, hep-ph/9510309
- [15] M. E. Peskin, Int. J. Mod. Phys. A 13 (1998) 2299, hep-ph/9803279
- [16] A. Pukhov et al., hep-ph/9908288
- [17] G. Altarelli, F. Caravaglios, G. F. Giudice, P. Gambino and G. Ridolì, J. High Energy Phys. 06 (2001) 018, hep-ph/0106029